

Closed-loop control of dielectric permittivity for 3D-printed radio-frequency devices

Sophie A. Lekas, Ross Drummond, Patrick S. Grant and Stephen R. Duncan

Abstract—Additive manufacturing (AM) offers significant advantages over traditional manufacturing methods for the fabrication of radio-frequency (RF) devices due to lower production costs, flexibility to produce complex geometries, and ability to vary the internal composition of a part. Because AM processes are typically run without any online feedback control, printed parts may be compromised by defects. This paper proposes a feedback control algorithm to enable closed-loop control of a graded-index (GRIN) RF lens produced using a Fused Filament Fabrication printer. As a GRIN lens relies on spatially-varying permittivity, differing densities were printed on a layer-by-layer basis, thus changing the permittivity through the lens depth. The control system used a split ring resonator to measure the permittivity of printed material, and the control action was applied by updating the printed infill density in each layer. The results indicate the controller could detect and adjust for errors, demonstrating the potential of closed-loop control for precise fabrication of high value-added RF devices.

I. INTRODUCTION

Additive manufacturing (AM), commonly referred to as 3D printing, is the process of creating a 3D object by depositing or solidifying material in layers, with each bonding to the previous layer. Compared to traditional subtractive manufacturing methods, such as computer numerical control (CNC) milling, AM offers a number of advantages such as reduced material waste and energy, lower prototyping costs and the ability to create otherwise impossible geometries. While AM has traditionally been used for rapid prototyping, it is used increasingly for the manufacture of high value-added parts in a range of industry applications requiring precision engineering, including lightweight machinery [1], medical devices [2] and aerospace structures [3].

Despite AM's many advantages, fabricating parts incrementally, layer-by-layer, also has limitations. In particular, producing parts in large numbers remains difficult due to long fabrication times and lack of online quality control. AM processes are generally implemented as an *open-loop* system where no information is collected about the part during printing. Therefore, the printer is unable to provide online fault detection and rejection. The lack of feedback control within the printing process can lead to poor quality parts, including variations in porosity, lack of interlayer bonding and poor surface finish. Several classes of disturbances have

been encountered within AM, as categorised by Oropallo and Piegl [4] who separated them into i) process errors (e.g. due to mechanical problems or improperly-set printing parameters) and ii) material errors (e.g. from variations in the feedstock caused by improper storage). Both types of error have been observed to cause printing imperfections that may propagate through subsequent layers (e.g. millimetre scale pores), and in some cases, ruining printed parts in their entirety. As AM parts are increasingly being used for industrial applications and safety-critical parts, there is a growing need to introduce systems capable of i) online fault detection and ii) corrective action. Feedback control has the potential to achieve both these objectives.

There has been significant work to apply closed-loop feedback control to AM processes. The design of an effective control policy relies upon a good predictive model of the system, which has motivated several recent results on control-oriented modeling of layer deposition/solidification [5]–[7]. The potential of various control methods have also been examined to control mechanical properties within 3D-printed parts. In [8], model predictive control was used to meet precise stiffness requirements of a printed beam, and [9] demonstrated the use of proportional-integral-derivative control to regulate deposition microstructure. In contrast, the current work instead focuses on controlling electromagnetic (EM) properties for radio-frequency (RF) devices—a novel application of feedback control in an AM process.

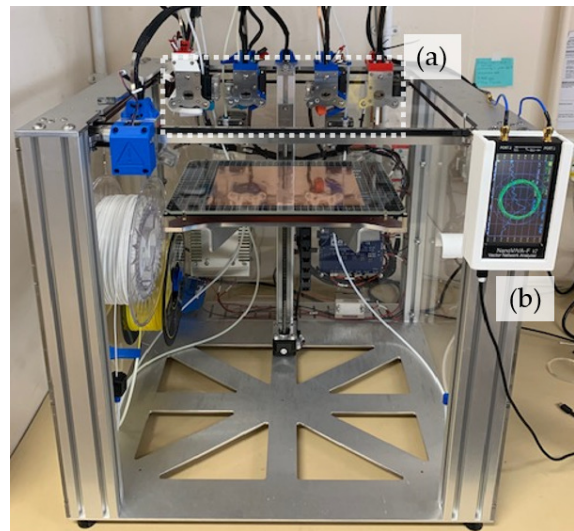


Fig. 1. Photograph of the ToolChanger & Motion System with (a) tools including extruders and the SRR device and (b) VNA attached to the frame.

Sophie A. Lekas, Ross Drummond, and Stephen R. Duncan are with the Department of Engineering Science, University of Oxford, Oxford OX1 3PJ, United Kingdom. Email: {sophie.lekas, ross.drummond, stephen.duncan}@eng.ox.ac.uk.

Patrick Grant is with the Department of Materials, University of Oxford, OX1 3PH Oxford, United Kingdom. Email: patrick.grant@materials.ox.ac.uk.

The EM property of interest is the complex dielectric permittivity ϵ , a measure of the electric polarizability of a dielectric material. When an electric field is applied, a material with high permittivity responds with higher polarization than a material with low permittivity, thereby storing more energy in the material. The relative permittivity ϵ_r of a medium is computed as the ratio of the permittivity of the medium ϵ to the absolute permittivity of the surrounding air or vacuum ϵ_0 [10]. The ability to use dielectric materials in AM has generated strong interest in 3D printing RF components used in optics [11], electronics [12] and communications [13].

AM offers a low-cost and accessible technique to create RF devices as the permittivity through an object can be varied by changing the spatial variation of printed material [14]. For example, graded-index (GRIN) lenses are an attractive alternative to classical lenses for antenna applications due to their flat design [15]. However, the development of GRIN lenses has been slow due to the challenges of conventional manufacturing approaches, often involving tightly fitting materials of differing EM properties together and very precise machining [16]. AM offers a solution to this; a 3D-printed GRIN lens has been formed using two materials with different relative permittivities that were mixed as a function of position [17]. Similarly in [18], a GRIN lens was fabricated by varying the permittivity of a single material; concentric circles of differing infill density were printed to vary the permittivity from the lens center to the perimeter.

While AM can fabricate a GRIN lens, limitations constrain its effectiveness. Neither lens in [17] nor [18] was able to achieve a continuous radial variation in permittivity due to the inability to continuously mix materials within a layer and the resolution of the printer, respectively, decreasing the focusing accuracy and achievable gain. This arose from the need to discretize the spatial distribution of permittivity into small “zones” of constant permittivity.

As most 3D printers currently have no process-monitoring or feedback system, they have no method of ensuring a printed part meets desired material properties, such as local permittivity [4]. They also cannot identify errors during printing, which can drastically affect a part. This lack of knowledge presents an opportunity for the application of control feedback into AM. The achievable quality improvements by the integration of a sensor and controller into a 3D printer for production of RF components are currently unknown.

Contributions: Within this context, the main results of this paper are:

- the design and construction of a Fused Filament Fabrication (FFF) 3D printer containing a sensor that measures the permittivity of just-printed polymer and a closed-loop control system;
- the characterization of the dielectric printed polymer components and a model describing the relationship between infill density and dielectric permittivity;
- the design of a proportional-integral (PI) controller for regulating the printed relative permittivity;
- an assessment of performance of the designed controller during the fabrication of a proof-of-concept GRIN lens.

The results demonstrate the potential for feedback control to improve the quality of 3D-printed GRIN lenses by enabling tighter part tolerances and online fault detection.

Paper structure: The paper is structured as follows. Section II details the physical construction of the printer hardware and sensor. Section III describes the system architecture of the printing workflow and data collection. Section IV presents the model identification and controller design process. Section V details the controller testing procedure, production of a proof-of-concept GRIN lens, and discussion of test results. Section VI provides concluding remarks.

II. PRINTING HARDWARE

A. 3D Printer

The printing system hardware used to conduct experiments is shown in **Fig. 1**. The hardware was designed with three main components: (i) an FFF printer, (ii) a sensor to measure permittivity and enable feedback, and (iii) a Vector Network Analyser (VNA) to generate and measure parameters associated with the dielectric sensor. FFF involves a continuous filament of thermoplastic material fed through a heated extruder nozzle that is deposited layer-by-layer. The *ToolChanger and Motion System* (E3D, Oxford, UK) was chosen as the FFF printer due to its open frame (allowing for easy modification) and extensive tool-changing ability. The *Motion System* contained a solid frame surrounding a 200mm x 300mm x 300mm build volume. It was controlled by the *Duet2 WiFi Controller Board*, a 32 bit processor that allowed either network or USB connectivity and ran on open source *RepRapFirmware*. Using a pickup and drop-off action, the *ToolChanger* allowed for up to four multi-function tools (e.g. print-head, laser, or inspection camera) to be utilised during a single print. For the experiments described in this paper, the *ToolChanger* was fitted with a Direct Drive Hemera hot-end (V6 0.4mm brass nozzle, E3D, Oxford, UK) as well as a compact dielectric sensor (see following section) that could be moved through the build volume.

B. Sensor Design

In order to implement online feedback control to regulate the relative permittivity ϵ_r through a 3D-printed part, a sensor is required that is capable of making measurements

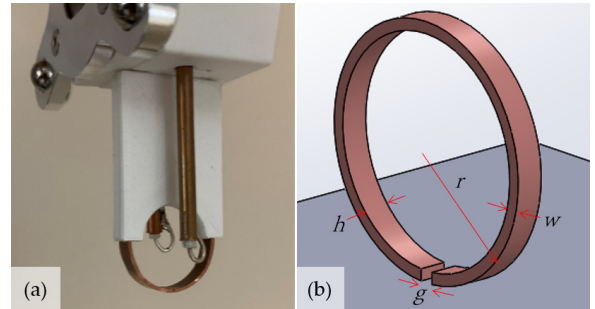


Fig. 2. (a) The split-ring and two magnetic loops held in place with a 3D-printed case. (b) Model of the SRR dimensions: width w , height h , outer radius r , and gap width g .

of each printed layer. Any acceptable sensor is required to be both non-destructive and able to operate in-situ, i.e. during the printing process. To satisfy these criteria, a splitting resonator (SRR) device was selected as the sensor due to its ability to take measurements layer-to-layer and map the local relative permittivity within a 3D-printed part, as demonstrated in [19]. The SRR device was formed by placing two magnetic loops equidistant from a split ring (illustrated in **Fig. 2**) so as to produce an electric field, causing the split ring to resonate at a frequency f_0 . The resonant frequency of the split-ring in air $f_{0,\text{air}}$ can be modelled as an LC circuit

$$f_{0,\text{air}} = \frac{1}{2\pi\sqrt{LC_{\text{tot}}}} \quad (1)$$

with effective inductance L and total capacitance C . The total capacitance

$$C_{\text{tot}} = C_{\text{gap}} + C_{\text{ring}} \quad (2)$$

is the sum of the capacitance across the split in the ring C_{gap} and the capacitance of the ring surface C_{ring} [20]. The parameters C_{gap} , C_{ring} and L , are characterised by the ring geometry (in particular, the width w , height h , outer radius r , and gap width g , depicted in **Fig. 2b**) and using relationships from [21], can be calculated using

$$C_{\text{gap}} = \varepsilon_0 \left(\frac{hw}{g} \right) + \varepsilon_0(h + w + g), \quad (3a)$$

$$C_{\text{ring}} = 2\varepsilon_0 \left[\frac{h+w}{\pi} \ln \left(\frac{4r}{f} \right) \right], \quad (3b)$$

$$L = \mu_0 r \left[\ln \left(\frac{8R_m}{h+w} \right) - \frac{1}{2} \right], \quad (3c)$$

where ε_0 and μ_0 are the free-space permittivity and permeability and $R_m = r - \frac{h}{2}$ is the mean ring radius. When a material of relative permittivity greater than air, so that $\varepsilon_r > 1$, is placed close to the SRR gap ($< 0.5\text{mm}$), the induced electric field across the gap is distorted, resulting in a measurable shift in resonant frequency f_0 . It is this distortion that is exploited in this work to measure EM properties online and enable feedback control. Following the experimental results conducted in [22], the Δf_0 of the SRR has been shown to follow a logarithmic dependency upon the material's relative permittivity ε_r , so that it satisfies

$$\frac{\partial f_0}{\partial \varepsilon_r} = \frac{M_e}{\varepsilon_r} \quad (4)$$

where M_e is a best-fit coefficient dependent on the SRR's geometry. The SRR's resonant frequency f_0 is also known to depend upon the gap-material distance; the closer the material is to the gap, the stronger its influence on f_0 . Following [22], this relationship between f_0 and gap-material distance q is governed by

$$\frac{\partial f_0}{\partial q} = \frac{e^{M_q q^n}}{q^{1-n}} \quad (5)$$

where $n = 0.1$ and $M_q < 0$ is another best-fit coefficient. By combining equations (4) and (5), an expression relating the local permittivity of the material near the gap to both the

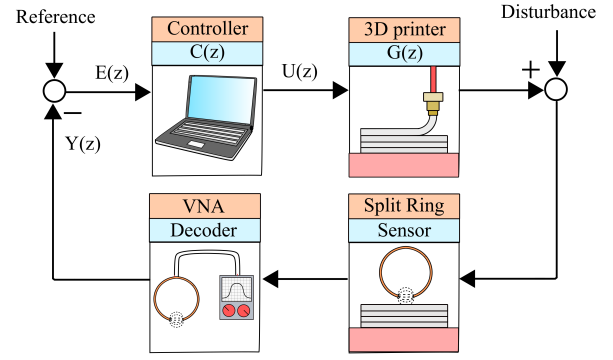


Fig. 3. Illustration of the feedback loop used to implement online control of the permittivity of the GRIN lens.

shifted SRR resonant frequency and gap distance is obtained

$$\varepsilon_r = \exp \left(\frac{f_{0,\text{air}} - f_{0,\text{material}}}{M_e \exp(M_q q^{0.1})} \right) \quad (6)$$

where $f_{0,\text{material}}$ is the SRR's shifted resonant frequency in the presence of a material with separation $q = 0.2\text{mm}$.

C. Fabrication of the SRR

The SRR probe used in this paper was built in-house. The two magnetic loops of the SRR were fabricated by bending the inner conductor of a copper semi-rigid coaxial cable (RG402, Farnell, Leeds, UK) into a loop and soldering the end onto its outer conductor. SMA 50Ω male connectors were soldered onto the other end of the RG402 cables. The two magnetic loops were placed equidistant from a single copper split ring and held in place by a 3D-printed case. The case was designed to be printable and compatible with the *ToolChanger*, allowing the SRR to be swapped in and out during the printing process (**Fig. 2a**).

A NanoVNA-F V2 Portable VNA (SYSJOINT, Hangzhou, China) was used to extract the resonant frequency measurements of the SRR (**Fig. 1b**). Both transfer and receive ports were connected to the SRR's RG402 cables with straight 50Ω SMA-female to SMA-female adapters.

III. SYSTEM ARCHITECTURE

The *ToolChanger* was run with the compatible DuetWebControl (DWC), a web-based user interface for electronics running on Duet boards. Connecting over a network, the DWC allows control over the printer, including setting tool temperatures, running macro and print files, homing/moving each axis, and initiating printing. The DWC communicates with the printer using RepRap-style G-code, a programming language used primarily for the control of CNC machines. While the DWC was found to be a comprehensive user interface for operating the *ToolChanger*, difficulties were encountered in using it to communicate with other devices in the hardware, such as the VNA. For this reason, a custom printing host was coded to enable a multi-device printing process capable of taking with measurements between layers.

The code for the printing host was written in MATLAB because of its capability for interfacing with serial devices

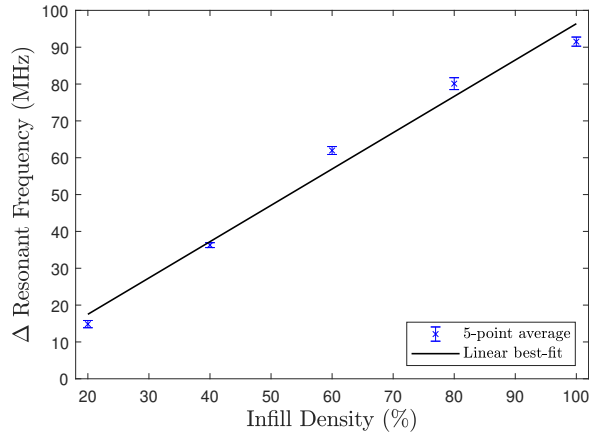


Fig. 4. The effect of infill density on the SRR's Δf_0 in proximity ($d = 0.2\text{mm}$) to PLA.

and micro-controllers. The G-code, used to set the printing parameters and divide the 3D model into individual thin layers, was produced using “PrusaSlicer” slicing software. Implementing online feedback control on a layer-by-layer basis required re-slicing the model upon each layer.

The printing host also managed the process workflow by initiating operations, either with the *ToolChanger* to print a layer and move the SRR, or with the VNA to take frequency measurements, as shown in **Fig. 3**. Serial connections from a laptop to both objects allowed simultaneous control and timing through the workflow. All data collected was stored in a structured array and processed after printing had been completed.

IV. CONTROLLER DESIGN

The first step in the design of the feedback control algorithm was to select an actuation mechanism that could correct for perturbations in the local permittivity of each layer. Here, the focus was on controlling the relative permittivity of parts formed from printed polylactic acid (PLA, $\epsilon_r \approx 3$), as measured by the change in SRR resonant frequency. Three printing parameters were tested for their sensitivity in controlling the local permittivity: (i) infill density, the percentage of interior volume that is filled with material; (ii) layer height, the thickness of a single layer; and (iii) extrusion width, the width of the line that is extruded from the nozzle. Of these, infill density was observed to perform best, giving the largest range in achievable shifts in the resonant frequency (and hence greatest level of control) while also following a simple relationship, as illustrated in **Fig. 4**. This relationship is approximated by the affine mapping

$$\Delta f_0 = m(\text{Infill Density}) + b \quad (7)$$

with $m = 0.986$ and $b = -2.213$. These features resulted in the variations in infill density being selected as the actuator used to implement the feedback control action.

A. Data-driven model

To design a feedback controller of the 3D printing process, a model was required to predict how changes in the infill

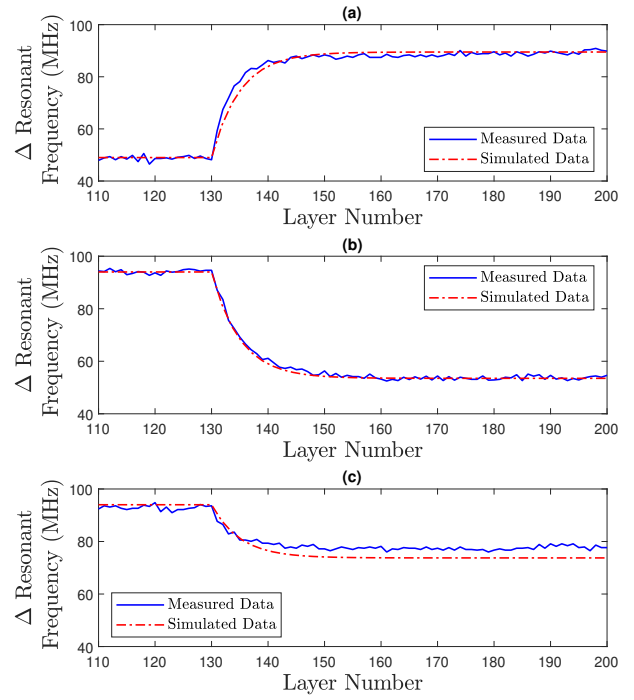


Fig. 5. Results from model-identification tests. (a) A positive step change of 40% infill density. (b) A negative step change of 40% infill density. (c) A negative step change of 20% infill density.

density (the control actuator) would affect the SRR Δf_0 (the model state being controlled). From inspecting the experimental data of open-loop step responses, shown in **Fig. 5**, it was observed that the layer-by-layer dynamics followed a first-order response. For that reason, a model of the form

$$G(z) = \frac{Y(z)}{U(z)} = \frac{az + b}{z + c} \quad (8)$$

was proposed where $Y(z)$ is the measured SRR frequency and $U(z)$ is the infill density used in the z -domain, with z corresponding to a single layer. For layer k , the model of Equation (8) implies the change in frequency satisfies the following recursion relationship

$$\Delta f_0[k + 1] = -c\Delta f_0[k] + au[k + 1] + bu[k]. \quad (9)$$

By estimating the system's time constant and steady-state values from the data of **Fig. 5**, the parameter values of $a = 0.09205$, $b = a$, $c = -0.8182$ were estimated for this model.

B. Controller calibration

A proportional-integral (PI) controller was used to provide feedback control on the local layer permittivity. This controller has the form (with $E(z)$ being the difference between the reference and desired Δf_0)

$$C(z) = \frac{U(z)}{E(z)} = k_P + \frac{k_I}{2} \left(\frac{z + 1}{z - 1} \right). \quad (10)$$

The gain values $k_P = 1$, $k_I = 0.25$ were calculated after manual tuning to deliver a non-overshooting closed-loop response and a sufficiently fast settling time of ≈ 17 layers.

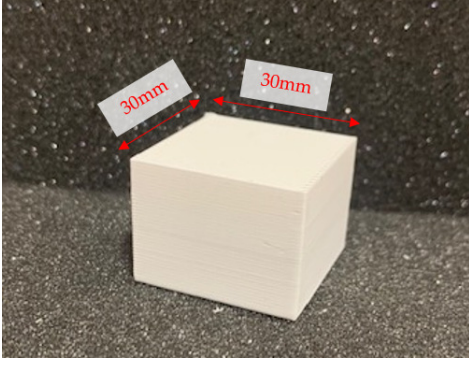


Fig. 6. The part produced from controller tests. Each test printed the same base dimensions with varying infill densities through the part's height.

V. RESULTS AND DISCUSSION

The algorithm was implemented on printed rectangular prisms (**Fig. 6**) with base dimensions of 30mm \times 30mm formed from the PLA whose properties were characterised in Section IV. No control action was implemented for the first 100 layers (system running in open loop), so as to remove the influence of the print bed on the SRR measurements. At layer 100, the control action was then turned on, with the SRR taking measurements after each printed layer.

A. Step responses

The first test of the controller explored its potential to mitigate the impact of step changes. The results are shown in **Fig. 7** for a positive and negative step change in reference Δf_0 , with **Fig. 7b** showing the change in the infill printed at each layer and the control signal. A noticeable error between the measured and desired resonant frequencies was observed

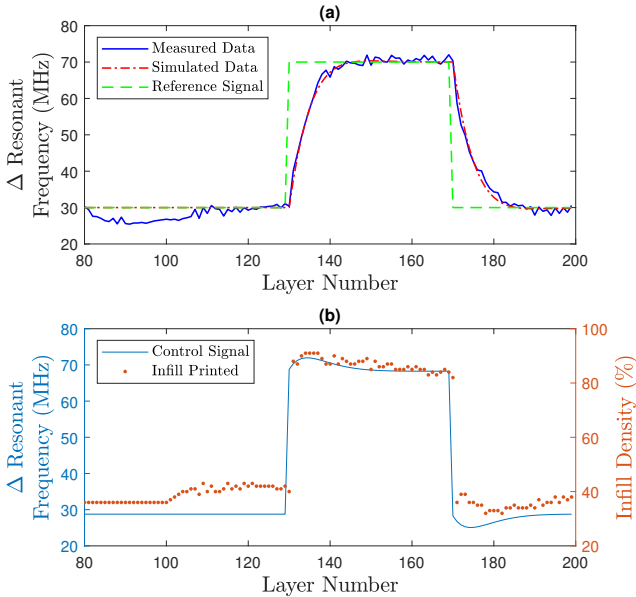


Fig. 7. Results of a positive and negative step change introduced using closed-loop control. (a) The measured Δf_0 shown against the reference signal and simulated controller response. (b) The infill density being adjusted after layer 100 in response to the control action.

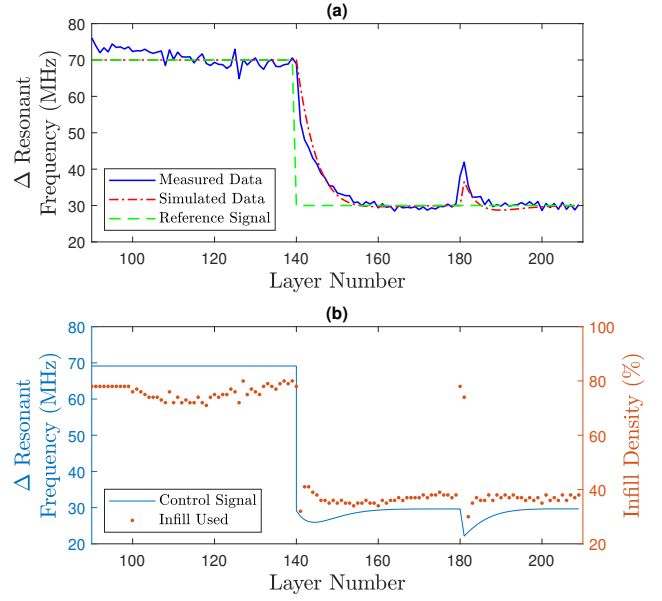


Fig. 8. Results of a negative step change, followed by an impulse disturbance. (a) The measured Δf_0 shown against the reference signal and simulated controller response. (b) The infill density being adjusted after layer 100 in response to the control action.

when the system was running open-loop, i.e. before the control algorithm was initiated at layer 100. After layer 100, Δf_0 reached the correct steady state value in ≈ 15 layers, demonstrating the ability of the algorithm to improve part accuracy and to accommodate sudden changes. The changing infill density control action applied by the algorithm (**Fig. 7b**) shows the initial open-loop response followed by the corrections implemented to achieve the feedback control. It is also noted that because the control scheme includes integral action, there was no steady-state error in the response.

The closed-loop experimental data of **Fig. 7** also show better correlation with the simulated response in comparison to the open-loop model simulations from Section IV, with the small error between these responses reinforcing the relative accuracy of this simple model.

B. Pulse disturbance

Process and material errors (described in Section I) can cause inconsistencies while printing, therefore creating a pulse disturbance in measured Δf_0 . The ability of the proposed controller to reject such a pulse disturbance was examined by manually introducing a differing infill density at a single layer. The results of this test are shown in **Fig. 8** for the case of a pulse disturbance of 80% infill density inserted at layer 180. These results again show the ability of the control system to quickly and automatically detect disturbances and then apply corrective feedback to limit its impact on the printed part, both once the controller is turned on at layer 100 and after the negative step change. It is also observed that the control system detected the disturbance and provided correcting action so as to remove its influence, returning the Δf_0 measurements to their desired steady-state of 30MHz. These results highlight the potential of the

controller for online fault detection and disturbance rejection.

C. GRIN Lens

Building upon the results of the step response and pulse disturbance, the performance of the control algorithm for manufacturing GRIN lenses was then evaluated. For this work, a proof-of-concept GRIN lens made from PLA was designed with a constantly-varying relative permittivity. The results, represented in **Fig. 9**, show the constant corrections made by the controller. The measured values of Δf_0 were in good agreement with the reference signal, demonstrating that a GRIN lens with specific changes in permittivity could be produced using this method. However, there was a delayed response in SRR measurements of ≈ 6 layers due to the influence of previous layers on the SRR's resonant frequency. Future work will explore removing this delay using feedforward control.

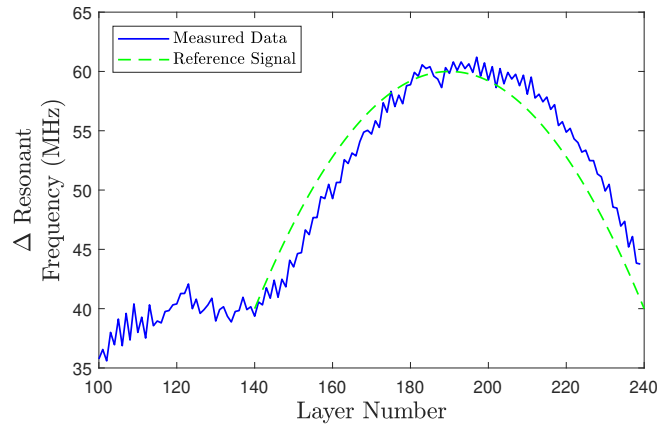


Fig. 9. Results of proof-of-concept GRIN lens fabrication.

VI. CONCLUSIONS

The successful implementation of feedback control in an FFF printer was used to produce a proof-of-concept GRIN lens, with a pre-designed spatial variation of relative permittivity, in good agreement to the reference design. The lens was limited to a range of permittivities between air ($\epsilon_r = 1$) and PLA ($\epsilon_r \approx 3$), but feedstock using composite materials with higher values of ϵ_r will increase design flexibility further. Although the preliminary model here used limits of allowable infill densities (20-100%), Model Predictive Control could be used to address these constraints. As a continuation of this research, another GRIN lens design will be manufactured in a single, controlled process, and then tested with an RF antenna to quantify and verify the benefits of a GRIN lens fabricated with process control.

ACKNOWLEDGMENT

Ross Drummond acknowledges the Royal Academy of Engineering for funding through a UKIC fellowship. This work was supported by the Nextrode project, funded by the Faraday Institution [grant number FIRG015]. For the purpose of Open Access, the author has applied a CC BY public

copyright licence to any Author Accepted Manuscript version arising from this submission.

REFERENCES

- [1] K. V. Wong and A. Hernandez, "A review of additive manufacturing," *International Scholarly Research Notices*, vol. 2012, 2012.
- [2] M. Javaid and A. Haleem, "Additive manufacturing applications in medical cases: A literature based review," *Alexandria Journal of Medicine*, vol. 54, no. 4, pp. 411–422, 2018.
- [3] J. C. Najmon, S. Raeisi, and A. Tovar, "Review of additive manufacturing technologies and applications in the aerospace industry," *Additive Manufacturing for the Aerospace Industry*, pp. 7–31, 2019.
- [4] W. Oropallo and L. A. Piegler, "Ten challenges in 3D printing," *Engineering with Computers*, vol. 32, no. 1, pp. 135–148, 2016.
- [5] E. C. Balta, D. M. Tilbury, and K. Barton, "Layer-to-layer stability of linear layerwise spatially varying systems: Applications in fused deposition modeling," *IEEE Transactions on Control Systems Technology*, vol. 29, no. 6, pp. 2517–2532, 2021.
- [6] S. Koga, M. Krstic, and J. Beaman, "Laser sintering control for metal additive manufacturing by pde backstepping," *IEEE Transactions on Control Systems Technology*, vol. 28, no. 5, pp. 1928–1939, 2020.
- [7] P. Hagqvist, A. Heralić, A.-K. Christiansson, and B. Lennartson, "Resistance based iterative learning control of additive manufacturing with wire," *Mechatronics*, vol. 31, pp. 116–123, 2015.
- [8] K. Garanger, T. Khamvilai, and E. Feron, "Validating feedback control to meet stiffness requirements in additive manufacturing," pp. 2053–2060, 2020.
- [9] M. H. Farshidianfar, A. Khajepour, and A. Gerlich, "Real-time control of microstructure in laser additive manufacturing," *The International Journal of Advanced Manufacturing Technology*, vol. 82, no. 5-8, pp. 1173–1186, 2016.
- [10] V. Monebhurrn, "IEEE standard 211-2018: IEEE standard definitions of terms for radio wave propagation," *IEEE Antennas and Propagation Magazine*, vol. 61, no. 3, pp. 126–126, 2019.
- [11] K. Willis, E. Brockmeyer, S. Hudson, and I. Poupirev, "Printed optics: 3D printing of embedded optical elements for interactive devices," in *Proceedings of the 25th annual ACM symposium on User interface software and technology*, 2012, pp. 589–598.
- [12] H. Yang, W. R. Leow, and X. Chen, "3d printing of flexible electronic devices," p. 1700259, 2018.
- [13] J. Kimionis, M. Isakov, B. S. Koh, A. Georgiadis, and M. M. Tentzeris, "3D-printed origami packaging with inkjet-printed antennas for rf harvesting sensors," *IEEE Transactions on Microwave Theory and Techniques*, vol. 63, no. 12, pp. 4521–4532, 2015.
- [14] H. Hu, S. Sinha, N. Meisel, and S. G. Bilén, "Permittivity of 3D-printed nylon substrates with different infill patterns and densities for design of microwave components," *Designs*, vol. 4, no. 3, p. 39, 2020.
- [15] J. Suszek, A. Siemion, M. S. Bieda, N. Błocki, D. Coquillat, G. Cywiński, E. Czerwińska, M. Doch, A. Kowalczyk, N. Palka *et al.*, "3D-printed flat optics for THz linear scanners," *IEEE transactions on Terahertz Science and Technology*, vol. 5, no. 2, pp. 314–316, 2015.
- [16] R. K. Arya, S. Zhang, Y. Vardaxoglou, W. Whittow, and R. Mittra, "3D-printed lens antenna," in *2017 IEEE International Symposium on Antennas and Propagation & USNC/URSI National Radio Science Meeting*. IEEE, 2017, pp. 7–8.
- [17] D. Isakov, C. J. Stevens, F. Castles, and P. S. Grant, "3D-printed high dielectric contrast gradient index flat lens for a directive antenna with reduced dimensions," *Advanced Materials Technologies*, vol. 1, no. 6, p. 1600072, 2016.
- [18] S. Zhang, R. K. Arya, S. Pandey, Y. Vardaxoglou, W. Whittow, and R. Mittra, "3D-printed planar graded index lenses," *IET Microwaves, Antennas & Propagation*, vol. 10, no. 13, pp. 1411–1419, 2016.
- [19] L. Fieber, S. S. Bukhari, Y. Wu, and P. S. Grant, "In-line measurement of the dielectric permittivity of materials during additive manufacturing and 3D data reconstruction," *Additive Manufacturing*, vol. 32, p. 101010, 2020.
- [20] D. Isakov, C. Stevens, F. Castles, and P. Grant, "A split ring resonator dielectric probe for near-field dielectric imaging," *Scientific Reports*, vol. 7, p. 2038, May 17, 2017.
- [21] O. Sydoruk, E. Tatartschuk, E. Shamonina, and L. Solymar, "Analytical formulation for the resonant frequency of split rings," *Journal of applied physics*, vol. 105, no. 1, p. 014903, 2009.
- [22] L. Fieber, "A hybrid additive manufacturing framework for the multi-phase fabrication and in-line characterization of functional devices," Ph.D. dissertation, University of Oxford, 2020.